Neural Network Configuration and Efficiency Underlies Individual Differences in Spatial Orientation Ability

Aiden E. G. F. Arnold, Andrea B. Protzner, Signe Bray, Richard M. Levy, and Giuseppe Iaria

Abstract

■ Spatial orientation is a complex cognitive process requiring the integration of information processed in a distributed system of brain regions. Current models on the neural basis of spatial orientation are based primarily on the functional role of single brain regions, with limited understanding of how interaction among these brain regions relates to behavior. In this study, we investigated two sources of variability in the neural networks that support spatial orientation—network configuration and efficiency—and assessed whether variability in these topological properties relates to individual differences in orientation accuracy. Participants with higher accuracy were shown to express greater activity in the right supramarginal gyrus, the right precentral cortex, and the left hippocampus, over and above a core network engaged by the whole group. Additionally, high-performing individuals had increased levels of global efficiency within a resting-state network composed of brain regions engaged during orientation and increased levels of node centrality in the right supramarginal gyrus, the right primary motor cortex, and the left hippocampus. These results indicate that individual differences in the configuration of task-related networks and their efficiency measured at rest relate to the ability to spatially orient. Our findings advance systems neuroscience models of orientation and navigation by providing insight into the role of functional integration in shaping orientation behavior. ■

INTRODUCTION

The ability to spatially orient within an environment is a complex behavior producing a high amount of interindividual variability in performance (Arnold et al., 2013; Liu, Levy, Barton, & Iaria, 2011; Wolbers & Hegarty, 2010). Spatial orientation is a highly integrative skill, requiring processing from brain systems underlying attention, working memory, object recognition, and decision-making (Harvey, Coen, & Tank, 2012; Bolognini, Olgiati, Rossetti, & Maravita, 2010; Arleo & Rondi-Reig, 2007; Corbetta, Kincade, & Shulman, 2002). To date, much of the work done in modeling the neurocognitive processes underlying spatial orientation has focused on the functional specialization of particular brain regions engaged during orientation within a navigation-related network (Wolbers & Büchel, 2005; Hartley, Maguire, Spiers, & Burgess, 2003; Iaria, Petrides, Dagher, & Pike, 2003; Maguire et al., 1998). For example, in a recent study by Marchette, Bakker, and Shelton (2011), individual differences in navigation behavior were examined using an ROI analysis that focused on bilateral hippocampus and bilateral caudate nucleus. The researchers found that the proportion of engagement in the hippocampus relative to the caudate nucleus was related to the use of a flexible cognitive mapping style, rather than a more rigid route following style. Although the results offer a compelling perspective on a long-standing debate about place versus response spatial learning in humans, the authors note that they believe both the hippocampus and the caudate nucleus are situated within broader memory and learning networks and that the ROI analysis should be interpreted in the context of these networks.

Systems neuroscience models (Burgess, 2008; Byrne, Becker, & Burgess, 2007; Burgess, Becker, King, & O'Keefe, 2001) based on these and similar studies have attempted to provide a network topology by proposing a computational framework for how regions within the brain are hypothesized to interact during spatial orientation. In these models, emphasis is placed on the dynamic interplay of brain regions contained primarily in the parietal cortices and the medial-temporal lobes, which are believed to process egocentric and allocentric spatial reference frames, respectively. During spatial orientation and navigation, an individual must dynamically coordinate information being processed in this network, suggesting that variability in topological characteristics may influence a person's ability to perform spatial tasks. However, to our knowledge, no empirical work has been done to examine whether different topological characteristics of these networks in humans relate to individual differences in orientation performance.

In this study, we address this issue by identifying two sources of variability in large-scale neural networks—network configuration (i.e., which brain areas are included

University of Calgary

Journal of Cognitive Neuroscience 26:2, pp. 380–394
doi:10.1162/jocn_a_00491

in a task-related network) and network efficiency (i.e., how effective are brain areas in a network at integrating information)—and investigating their relationship to individual differences in spatial orientation. Specifically, we investigated whether individuals engage different patterns of brain activity depending on their ability to accurately orient and whether the underlying functional architecture of these networks as measured by global efficiency and node centrality relate to accurate spatial orientation.

To achieve this, we identified the networks that support spatial orientation using a spatial orientation decision task (Arnold et al., 2013). Task-based fMRI was performed while individuals performed a series of orientation decisions, and these data were analyzed to identify brain regions engaged by the whole group as well as any individual differences in regional activity associated with performance differences on the orientation task. Resting-state MRI data that had been obtained before the task-based fMRI data were then examined to evaluate how effective these regions are at integrating information at a network level. We chose to focus on resting-state fMRI as it is believed to be a primary measurement of the brain's functional architecture (Biswal et al., 2010) and can be used in combination with the mathematical framework of graph theory to understand the capacity of brain networks to efficiently integrate information (van den Heuvel & Hulshoff Pol, 2010; Rubinov & Sporns, 2009). Previous studies using resting-state fMRI provide evidence for a link between brain network topology and individual differences in various cognitive processes, including perceptual learning (Baldassarre et al., 2012), working memory (Hampson, Driesen, Skudlarski, Gore, & Constable, 2006), intelligence (van den Heuvel, Stam, Kahn, & Hulshoff Pol, 2009), and the encoding of spatially relevant objects (Wegman & Janzen, 2011). This suggests that heterogeneity in resting-state fMRI signal used to measure the functional connectivity of spatially remote brain regions may provide an important metric for understanding the capacity of cognitive processes that rely on those regions.

METHODS

Participants

Sixteen healthy, right-handed volunteers (nine women, mean age = 22 years, age range = 18–36 years) with no psychiatric or neurological disorders and normal or corrected-to-normal vision participated in the study. All participants provided written informed consent as approved by the local research ethics board (CHREB 22848).

Behavioral Tasks

The experiment began with a spatial learning task conducted inside the MRI scanner. The spatial learning task was done to ensure that the participants formed a correct and stable mental representation of the spatial layout of the virtual city. All participants were given a verbal overview of the task and instructions for how to make proper responses before entering the scanner. During the spatial learning task, participants viewed nine 1-min video clips[1] of random passive movement in first-person perspective through a virtual city that included four unique landmarks in a 5 × 5 rectangular grid of identical buildings (Figure 1). They additionally viewed three control clips of a virtual city with no unique landmarks in a similar 5 × 5 rectangular grid. Experimental and control clips were presented in pseudorandom order: A control clip was presented at the start and end of the run, with nine experimental clips and one control clip presented in randomized order in between the control clips. ISIs between 4 and 6 sec were randomized between clips. To verify the correct spatial

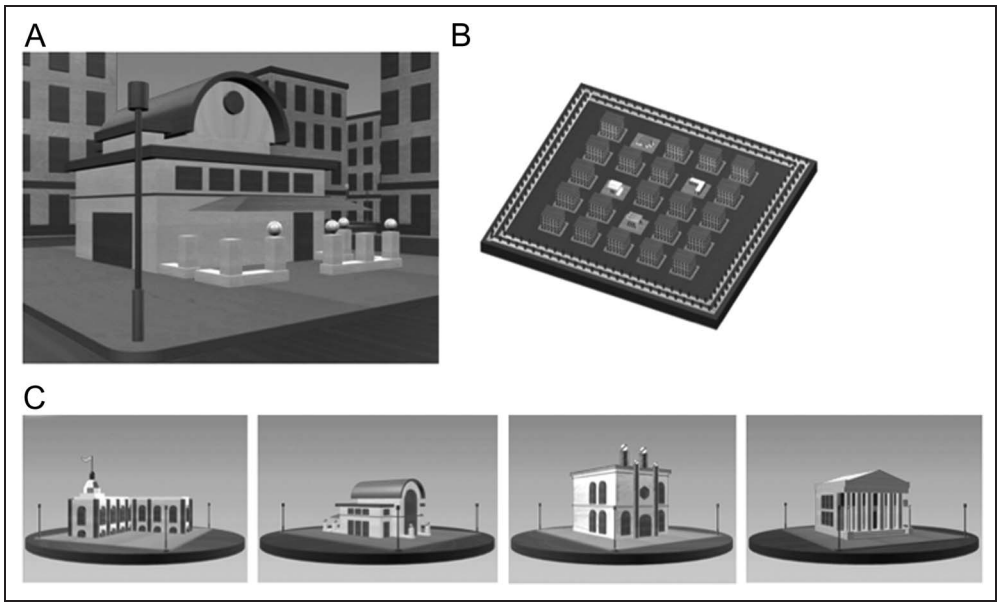

Figure 1. Stimuli set used during the learning (i.e., encoding) task. (A) Example of one of the landmarks as seen by the participants in the video clips from first-person perspective. (B) Aerial view of the 5 × 5 rectangular grid city on which participants indicated the location of each of the four landmarks encountered while navigating in the virtual city. (C) The four unique landmarks whose spatial arrangement within the city was encoded during the learning phase.

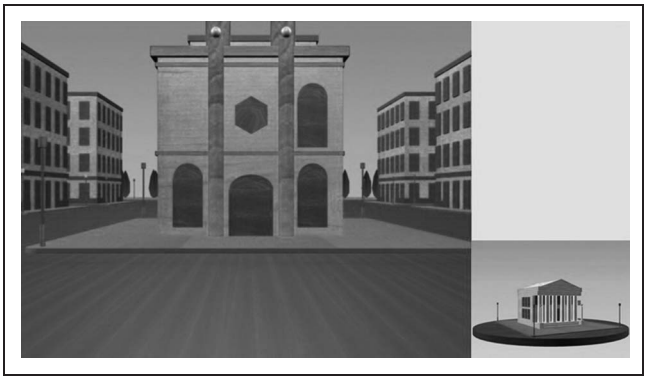

Figure 2. Stimulus presentation format for the orientation decision task. Participants indicated whether they should turn left or right from the view of the starting landmark (i.e., the building in central image) to get to the target landmark (i.e., the building on the right side) by following the shortest path possible.

encoding of the four landmarks within the virtual city, participants were asked to locate the position of each landmark on an aerial view of the 5 × 5 rectangular city grid once the scanning session was complete and they were removed from the scanner. This testing occurred between 20 and 40 min after exposure to the last experimental clip, depending on where in the testing sequence the spatial learning task was presented. Data from participants who were unable to correctly recall the spatial arrangement were excluded from all analyses.

Following the spatial learning task, participants performed an orientation decision task. Six experimental trials were randomized with six control trials within a single run. During experimental trials, participants saw the instructions "Left/Right" for 2 sec, followed by a fixation cross that jittered between 4 and 6 sec. This was followed by a central image of a ground-level view of one of the four landmarks with a second image displaying a second landmark on the right side of the screen (Figure 2). Before the run, participants were instructed to treat the central image as their starting point and the secondary image on the right side of the screen as their target destination. The secondary image presented a landmark without a background (i.e., devoid of visual context within the city). After image onset, participants had 10 sec to respond whether they should turn left or right to travel from the primary landmark to the secondary landmark by following the shortest path possible. Responses were made on a two-button Lumina response box (Cedrus Corporation, San Pedro, CA). An index finger button represented a left turn, and a middle finger button represented a right turn. All responses were made with the right hand. Trials in this task were randomized with control trials in which participants made perceptual judgments (i.e., is building A bigger or smaller than building B) about buildings that were visually similar but distinct from the landmarks encoded while exploring the virtual city.

Two additional control tasks were performed outside of the scanner and used to ensure that the network analysis results were specifically related to spatial orientation ability and not reflective of individual differences in other nonspatial perceptual processes. A face identity recognition task assessed each participant's ability to recognize the identity of human faces from different perspectives. It consisted of 12 trials that showed a grayscale photograph of a human face in frontal view for 2000 msec. All faces were taken from the Karolinska Database of Emotional Faces (Lundqvist & Litton, 1998). After the stimulus presentation, participants were shown grayscale photographs of four faces that had been rotated 45° from frontal view. Participants used a mouse to click on the rotated face they believed corresponded to the previously viewed face in frontal view. Next, an emotion recognition test assessed each participant's ability to recognize facial expressions. The presentation format was identical to the face identity recognition test with all faces taken from the Karolinska Database of Emotional Faces (Lundqvist & Litton, 1998). Participants were first shown a grayscale photograph of a human face depicting either happiness, sadness, disgust, or surprise. Four grayscale photographs of the one individual depicting each of the four emotions were shown, and participants were asked to select the photograph that expressed the target emotion viewed in the previous photograph.

MRI Data Acquisition

Participants were scanned using a 3T GE Signa scanner with an eight-channel head coil at the Seaman Family MR Research Centre at the University of Calgary. Both resting-state and task-based functional scans were acquired using a T2*-weighted EPI sequence (repetition time = 2500 msec, FOV = 24.0 cm, 3 × 3 × 3 mm voxels in interleaved acquisition, flip angle = 77). Resting-state scans were conducted before task-based scans for either 5 min (total volumes = 120, nine participants) or 10 min (total volumes = 240, seven participants). High-resolution 3-D anatomical images were acquired using a SPGR sequence (180 slices, FOV = 25.6 cm, 1 × 1 × 1 mm voxels, flip angle = 11). Lastly, 60 direction diffusion tensor images (DTI) were acquired using a 2-D spin echo sequence (repetition time = 8000 msec, FOV = 25.6 cm, bo = 1000, 64 slices). DTI data were not analyzed for this study.

Task fMRI Data Processing

Task-based fMRI data from the orientation decision task were preprocessed using SPM8 (Wellcome Department of Imaging Neuroscience, Institute of Neurology, UCL; www.fil.ion.ucl.ac.uk/). Data were corrected for movement by realigning to the first volume of each scan, resliced into a 2-mm isotropic voxel space, normalized to the Montreal Neurological Institute (MNI) EPI template using a 12-parameter affine transformation, and smoothed using an 8-mm FWHM Gaussian kernel.

Resting-state fMRI Data Processing

Resting-state fMRI data were preprocessed spatially using the same pipeline as the task-based fMRI data and temporally processed using the CONN functional connectivity toolbox (Whitfield-Gabrieli & Nieto-Castanon, 2012; www.nitrc.org/projects/conn). To control for cardiac and respiratory artifacts in the resting-state signal, the anatomical aCompCor method of signal regression (Chai, Nieto-Castañón, Öngür, & Whitfield-Gabrieli, 2012; Behzadi, Restom, Liau, & Liu, 2007) was carried out after segmenting the 3-D anatomical scans into gray matter, white matter, and CSF. This was computed by estimating orthogonal time series using a PCA of the BOLD signal from the white matter and CSF images. These temporal confounding factors were then treated as nuisance variables and regressed from the resting-state time series of each voxel in the gray matter for each participant. To further minimize spurious correlations, motion correction parameters from the spatial realignment were regressed out as nuisance variables, as was the average effect across each section (block convolved with a hemodynamic response function) for each participant. The residual time series data were then band-passed through a 0.01–0.001 Hz filter to isolate brain signal that had been used to evaluate global efficiency measures in resting-state networks (van den Heuvel et al., 2009). The time series for each ROI was computed by averaging the temporally filtered residual time series for each voxel within the ROI. Bivariate correlation matrices between each ROI time series were then calculated, and a Fisher transformation (inverse hyperbolic tangent function) was then applied at the single-subject level to normalize the distribution of bivariate correlation values.

Task-based fMRI Data Analyses

All fMRI data collected during task performance were analyzed using partial least squares (PLS). A task PLS was conducted on fMRI data collected during the orientation decision task to identify similarities or differences in brain activation for orientation decisions versus perceptual decisions. In addition to a task PLS, a behavior PLS was performed, linking orientation decision performance to brain activity during the decision task. Specifically, behavior PLS identified regions in which individual differences in activity correlated with individual differences in orientation performance.

Task PLS: Definition

Task PLS is a multivariate technique that uses singular value decomposition to identify distributed activity patterns or latent variables (LVs) that show similarities or differences between experimental conditions. Each LV contains three vectors. The first vector contains a singular value, which indicates the strength of the effect expressed by the LV. The remaining two vectors relate experimental design and brain activity. The experimental design vector contains task saliences, which indicate the degree to which each task is related to the brain activity pattern identified in the LV. These task saliences can be interpreted as the optimal contrast that codes the effect depicted in the LV. The brain activity vector contains voxel saliences. These are numerical voxel weights that identify the collection of voxels that, as a whole, are most related to the effects expressed in the LV. Note that for each LV, there is one salience per voxel that applies for all tasks. PLS is similar to other multivariate techniques, such as PCA, in that contrasts across tasks typically are not specified by the experimenter. Instead, the algorithm extracts LVs explaining the covariance between tasks and brain activity in order of the amount of covariance explained, with the LV accounting for the most covariance extracted first.

Statistical assessment is then conducted using permutation tests for the LVs and bootstrap estimations of the standard errors for voxel saliences. Permutation tests ensure that the patterns represented in each LV are sufficiently different from random noise (McIntosh, Bookstein, Haxby, & Grady, 1996) using sampling without replacement to reassign the order of conditions for each participant. PLS is then recalculated for each sample, and the frequency at which the permuted singular values exceed the observed singular values are computed. Five hundred permutations were used during the present analysis. If LVs are found to be statistically significant through permutation tests, they are interpreted as providing a meaningful depiction of voxel-level activity across the brain in relation to either an experimental condition in the case of a task PLS or a behavior in the case of a behavior PLS. In the results section summarizing our PLS findings, we report the p value associated with each LV that is obtained through permutation tests. Bootstrap estimations are then used to test the reliability of nonzero voxel saliences in the LVs that have been identified as significant in the permutation tests. This is done using sampling with replacement where experimental conditions are fixed for all participants. PLS is recalculated for each bootstrap test and saliences whose value expresses significant variability dependent on which participants are in the sample are treated as less reliable. No corrections for multiple comparisons are necessary because voxel saliences are computed in one mathematical step across the whole brain. Bootstrap ratios (BSRs) are proportional to z scores but are interpreted as a confidence interval with an approximate p value. Note that the p value associated with bootstrap estimations is different than the p value associated with permutation tests for each LV. For this manuscript, a threshold of 3.3 corresponding roughly to a 99.9% confidence interval or a p value less than .001 was designated for bootstrap estimations. Each figure depicting patterns of task-related activity is set at a BSR of 3.3 or higher. A thorough description of PLS's application to block designs in fMRI studies is documented

in McIntosh et al. (1996) and visual schematics of the step-by-step process in PLS is available in Krishnan, Williams, McIntosh, and Abdi (2011).

The clusters with dominant positive saliences from the task PLS analysis on fMRI data collected during the orientation decision task were extracted for use as network nodes in the graph theory analysis. Specifically, ROIs were extracted from clusters identified at a BSR of 3.3 (p = .001) and a cluster threshold of 10 voxels with a minimum distance of 10 mm between clusters. For those clusters that had multiple peak voxels with a BSR of greater than 3.3 and a minimum distance of 10 mm between peaks, the BSR was increased to allow for the discrimination between independent clusters in the same cortical region that may have had overlapping edges. The same extraction method was conducted on the clusters from the behavior PLS that had a significant positive relationship to accuracy in orientation decisions. In total, 12 positive voxel salience clusters were extracted from the task PLS analysis and 4 positive voxel salience clusters were extracted from the behavior PLS analysis.

Behavior PLS: Definition

Behavior PLS examines the correlations between a behavior measure and neural activity. The behavior measure of interest to the research presented here was accuracy in orientation decisions. The correlation between accuracy and the rest of the brain was computed across participants during the orientation decision task, resulting in a matrix containing a within-task brain–behavior correlation map. Singular value decomposition of the brain–behavior correlation matrix was carried out to produce three new matrices: singular values, task saliences, and the singular image of voxel saliences. As in task PLS, the singular value indicates the strength of the effect expressed by the LV. The variation across task saliences indicates whether a given LV represents a similarity or difference in the behavior–brain correlations across tasks. The voxel saliences give the corresponding spatiotemporal activity pattern. Statistical assessment is similar to that used for task PLS.

Graph Metrics: Definition

In this study, we assessed two graph metrics that have been shown to quantify important information pertaining to the underlying topological structure of functional brain networks. The first, global efficiency (Rubinov & Sporns, 2010; Latora & Marchiori, 2001), is calculated as the inverse average shortest path length from node n in graph G to all other nodes in the graph. Global efficiency is based on the measure of characteristic path length (Watts & Strogatz, 1998), which quantifies the average number of edges needing to be traveled between nodes in a graph. Short path lengths are associated with graphs where each node, on average, can be reached from any other node by traveling along a small number of edges. Each graph contains a single global efficiency value that indicates the integrative and communicative capacity of a network to share information (van den Heuvel & Hulshoff Pol, 2010; Bullmore & Sporns, 2009; Sporns, Honey, & Kötter, 2007). Global efficiency has been hypothesized as the superior method of assessing integration in a network compared with characteristic path length because of its robustness against the number of disconnected or remote nodes in a graph (Achard & Bullmore, 2007).

The second graph metric assessed was the closeness centrality. Closeness centrality is calculated similarly to global efficiency, except on a node-by-node basis rather than as an average across each node in the graph (Sporns et al., 2007; Freeman, 1979). Thus, each node n in graph G is given a unique closeness centrality value that indicates the inverse average path length to get from that node to any other node in the graph. A node with a high closeness centrality can efficiently reach any other node in a graph by way of shorter paths and may therefore play a larger role in integrating the information content within the graph. Closeness centrality has been hypothesized as a valuable metric to understand the relative importance of different nodes within a network to share information (Rubinov & Sporns, 2010; van den Heuvel & Hulshoff Pol, 2010; Sporns et al., 2007) as nodes with high centrality are typically classified as "hubs" that allow for the propagation of information between different subcomponents of a network.

Graph Theory Analysis on Resting-state MRI Data

Graph theory measures were computed using the CONN functional connectivity toolbox (Whitfield-Gabrieli & Nieto-Castanon, 2012) inside the SPM program shell. We used an iterative stepwise pipeline outlined by Bullmore and Sporns (2009) that involves four steps to assess both global efficiency of graphs based on resting-state fMRI data and the closeness centrality of nodes within those graphs.

First, network nodes were defined. For the first analysis assessing global efficiency on the task PLS network, we used the 12 clusters extracted from the output of the task PLS analysis. Eleven clusters were extracted at a BSR of 3.3, whereas the left precuneus cluster (MNI peak = −10, −56, 50) was placed at a higher BSR of 4.4 to separate the left and right hemisphere peaks within the cluster. For the second analysis assessing closeness centrality, we added the four clusters from the behavior PLS analysis to the original 12 clusters.

Second, we averaged the preprocessed BOLD signal for each voxel within our two sets of ROIs and used the Fisher transformed correlation between each ROI as a measure of association between each node. This characterized the degree of connectivity between each ROI to be used in later steps.

Third, we generated an association matrix between each node in the network and set a threshold of $r > 0.15$ for

each node to define an undirected graph (i.e., adjacency matrix), such that each ROI is associated with a node in the graph and the Fisher transformed r value between each node is used to create the edges within the network. Although thresholds are sometimes omitted (Bullmore & Sporns, 2009), one was included in the present analysis to characterize an adjacency matrix that had small-world organization (Watts & Strogatz, 1998). Small-world properties have been observed in macaque, cat, and human brain networks (Melie-García, Sanabria-Diaz, & Sánchez-Catasús, 2013; Ginestet & Simmons, 2011; Iturria-Medina, Sotero, Canales-Rodriguez, Aleman-Gomez, & Melie-Garcia, 2008; Iturria-Medina et al., 2007; Hilgetag & Kaiser, 2004; Sporns, Tononi, & Edelman, 2000) and are generally believed to be the underlying network structure of the human brain because of their processing efficiency and robustness against network perturbations (Achard & Bullmore, 2007; Bassett & Bullmore, 2006). Small-world properties occur when the global efficiency of a graph is greater than that of a lattice graph and local efficiency is greater than that of a random graph (Achard & Bullmore, 2007). Watts and Strogatz (1998) characterized lattice graphs as a graph exhibiting regularity such that each node is maximally connected to its nearest neighbors, but not connected to nodes at a greater distance (i.e., it has high clustering). This results in short path lengths between neighboring nodes, but high path lengths between distant nodes. Conversely, random graphs were characterized as graphs with short path lengths and low clustering, indicating that neighboring nodes were as likely to be connected as more distant nodes.

Fourth, we calculated the global efficiency for each participant by computing the average inverse shortest path length between node n to all other nodes in each set using the mathematical framework for ROI-level and network-level measures of global efficiency outlined by Whitfield-Gabrieli and Nieto-Castanon (2012). In terms of functional connectivity measures, paths represented sequences of statistical associations rather than information flow along an anatomical substrate. These associations were taken as a measure of a brain network's ability to rapidly integrate information from distant brain regions (van den Heuvel & Hulshoff Pol, 2010; Rubinov & Sporns, 2010). This allowed us to evaluate global efficiency across all nodes contained in each network and measure the closeness centrality of each network node.

After characterizing the average group effects in our sample, we examined the relationship between accuracy and global efficiency in the task PLS network. We performed a simple linear regression analysis inside of CONN using two orthogonal covariates composed of (a) the adjacency matrices for each individual (weighted as 0) and (b) the individual's accuracy score from the orientation decision task (weighted as 1). The analysis threshold was set to $p < .05$, and global efficiency values were calculated. This gave parameter estimates representing the magnitude of relationship between the global efficiency values of an individual and their accuracy on the orientation task. A similar method was carried out for the closeness centrality analysis, except that a false discovery rate was calculated using closeness centrality values for all nodes within the network and applied to correct for multiple comparisons.

RESULTS

Behavioral Performance

Thirteen participants (seven women, mean age = 21.77, age range = 18–36 years) of the 16 participants correctly recalled the location of each of the four landmarks from the spatial learning task after the delay period. The three participants who were unable to correctly encode and retain the spatial layout of the virtual city were excluded from all analyses. Immediately following the spatial learning task, the orientation decision task was performed. As predicted from previous studies (Arnold et al., 2013; Liu et al., 2011), participants displayed a high degree of interindividual variability in their ability to correctly make orientation decisions based on previously encoded spatial information ($M = 3.08$, $SD = 1.55$; RT $M = 4938$ msec, $SD = 1652$). Although the nature of the dichotomous scoring metric of the orientation decision task resembles an accuracy distribution similar to a distribution obtained by chance through random responses, the fact that all 13 participants included in the analysis were able to correctly encode and retain the spatial layout suggests that the accuracy measured here reflects natural variability in effortful spatial orientation. We identified no significant performance differences between genders, $t(11) = -0.90$, $p = .39$. Additionally, we found no significant correlation between accuracy and age of the participants, $r = 0.02$, $p = .94$.

Neural Basis of Orientation Decisions—Task PLS Analysis

A task PLS was performed to identify the brain regions that showed unique increases in voxel activity during the orientation decision task and the perceptual decision task. These results are summarized in Table 1 and Figure 3. Our permutation test identified one significant LV ($p < .01$) that discriminated orientation decisions from perceptual judgments. Dominant positive saliences—brain areas showing significant increased activity while making orientation decisions—with a BSR of 3.3 ($p < .001$) were found bilaterally within the precuneus, cerebellum, and retrosplenial cortex (RSC), within the right hemisphere in the lingual, parahippocampal, and angular gyrus, and within the left hemisphere in the middle frontal and occipital gyrus. The dominant negative saliences are included in Table 1 for the sake of completeness. However, we do not discuss these regions in the context of this article because we were specifically interested in

Table 1. Dominant Positive and Negative Saliences from the Decision-phase Task PLS

Peak Voxel Location	*x (mm)*	*y (mm)*	*z (mm)*	*BSR*
Dominant Positive Saliences				
Left middle frontal gyrus	−26	−4	58	8.5440
Right middle frontal gyrus	22	−6	50	7.7902
Right retrolimbic area	10	−44	6	3.9050
Left inferior parietal lobule	−36	−44	46	4.2175
Right parahippocampal gyrus	32	−44	−4	4.1618
Right cerebellum	48	−48	−46	4.9354
Right posterior cingulate	20	−54	20	6.3658
Left precuneus	−10	−56	50	5.8746
Left posterior cingulate	−16	−58	16	5.6839
Right cerebellum	34	−66	−30	4.4361
Left superior occipital gyrus	−42	−86	36	4.5429
Dominant Negative Saliences				
Left superior medial gyrus	−4	58	12	−5.4686
Right superior medial gyrus	6	54	48	−4.4795
Left inferior frontal gyrus	−46	40	−22	−4.4244
Left superior temporal gyrus	−58	4	−8	−5.8343
Right middle frontal gyrus	50	−4	60	−7.1648
Left precentral gyrus	−42	−8	60	−5.1407
Left SMA	−6	−16	56	−5.3296
Left precentral gyrus	−22	−18	76	−4.4998
Right precentral gyrus	22	−28	78	−5.9127
Left postcentral gyrus	−22	−40	70	−4.9987
Left middle temporal gyrus	−62	−40	2	−4.6722
Right cerebellum	46	−70	−26	−4.3582
Right middle temporal gyrus	58	−74	0	−4.6225
Left inferior occipital gyrus	−38	−76	−10	−6.6311
Left inferior occipital gyrus	−26	−94	−6	−6.0954
Right superior occipital gyrus	20	−98	20	−6.695
Left superior occipital gyrus	−10	−98	34	−5.1141

These regions showed unique increases in BOLD activity while making orientation decisions. Peak voxels for each cluster are reported in MNI coordinates. Coordinates reported in MNI space.

examining the neural dynamics among regions in which activity increases during spatial orientation.

Global Efficiency within a Functionally Defined Orientation Network

A graph theoretical analysis was then conducted using 12 clusters extracted from our task PLS (see Methods) that were uniquely associated with making orientation decisions. Global efficiency values were calculated using resting-state fMRI data by creating using the 12 clusters. Global efficiency was then regressed against accuracy in the orientation decision task. This analysis is summarized in Figure 4. The results of this analysis were significant, $t(11) = 4.62, p < .001, R^2 = 0.66$, indicating that increased global efficiency within this network supported more

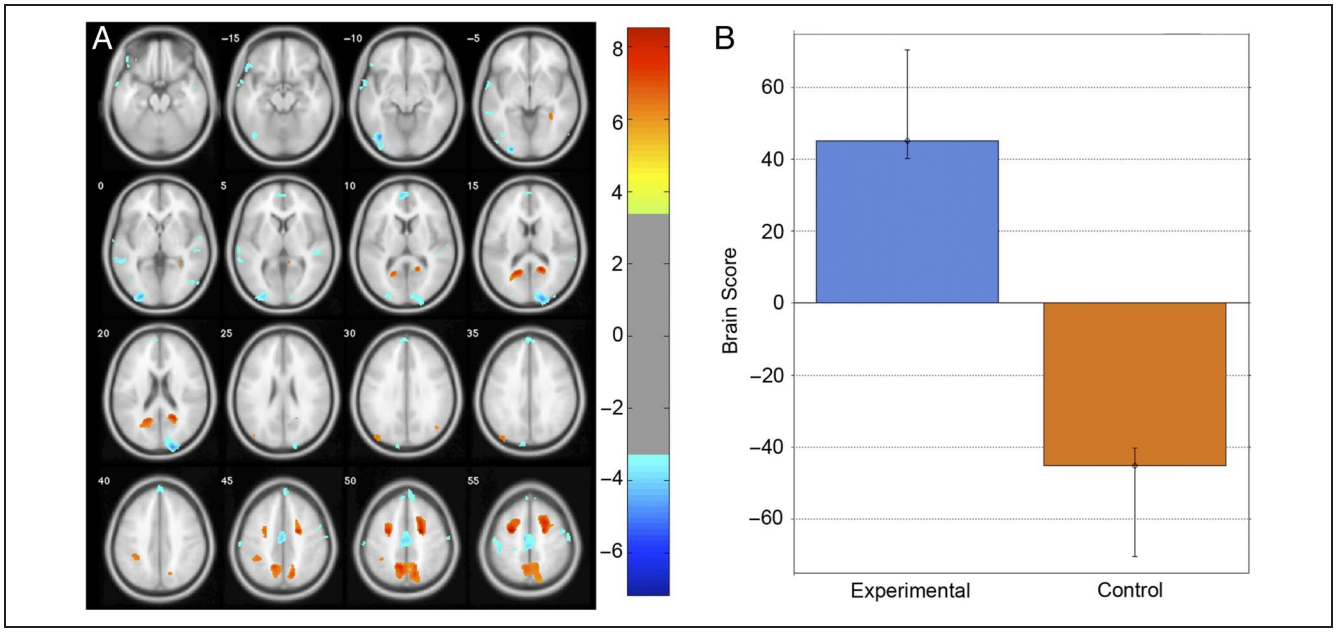

Figure 3. Singular image for the LV ($p < .01$) from the orientation decision task PLS. (A) Red/yellow regions represent increased activity while participants made orientation decisions based on viewpoint specific spatial information. Blue/green regions represent increased activity while making perceptual judgments of novel buildings. (B) Bar graph showing mean brain score for each task condition with associated confidence interval. Brain scores indicate the degree to which each participant shows the spatial pattern of voxels expressed in the LV. Displayed in neurological convention (L = L).

accurate orientation decision-making. Differences in global efficiency within this network were not related to gender (women: $M = 0.61$, $SD = 0.06$; men: $M = 0.63$, $SD = 0.14$), $t(11) = 0.29$, $p = .78$, or the age of participants, $r = -0.05$, $p = .88$.

Previous research has shown that global efficiency in frontal and parietal subnetworks measured through resting-state fMRI signal is related to scores on the performance IQ subscale of the WAIS III test (van den Heuvel et al., 2009). This suggests that global efficiency in certain resting-state subnetworks may have a generalized influence on nonverbal, perceptual reasoning tasks. To ensure that our results were specific to spatial orientation and did not relate to other nonspatial perceptual skills, we assessed the relationship between global efficiency values derived from this task-based network with performance on a face identity task and an emotion recognition task using a regression analysis. Global efficiency of the orientation decision network was not significantly related to performance on the face identity task, $t(11) = -1.27$, $p = .88$, $R^2 = 0.15$, or the emotion recognition task, $t(11) = -0.45$, $p = .67$, $R^2 = 0.02$. These results

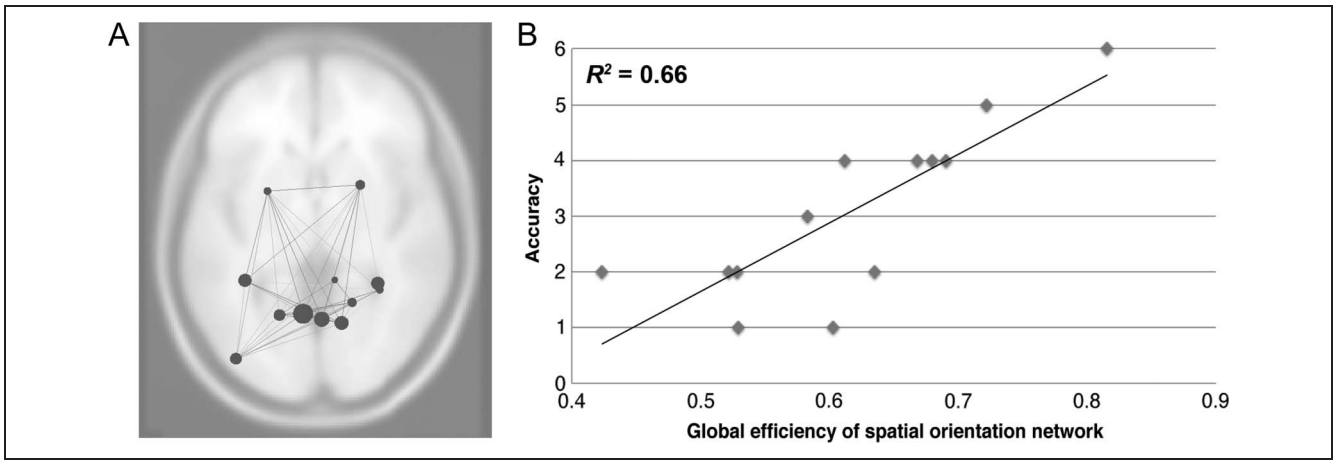

Figure 4. Overview of global efficiency results in the task PLS network. (A) Axial view of task-defined resting-state network. Size of dot represents degree of centrality for each node in the network. (B) Regression plot showing relationship between accuracy in making orientation decisions and global efficiency in all nodes in the functionally defined decision network, $t(11) = 4.62$, $p < .001$, $R^2 = 0.66$.

suggest that global efficiency within the task-defined network is specific to spatial orientation and does not appear to generalize to nonspatial perceptual tasks.

Neural Basis of Interindividual Variability in Orientation Decisions—Behavior PLS

Although the results from the task PLS identified a core set of brain regions that showed unique increases in activity during the orientation task across the whole group, we further decomposed the task fMRI data to investigate whether high-performing individuals engaged additional brain regions over and above this set of regions. To achieve this, we conducted a behavior PLS on the orientation decision task fMRI data. These results are summarized in Table 2 and Figure 5. Our permutation test identified a single significant LV ($p < .05$) that showed brain regions that were more active in the context of greater accuracy on the orientation decision task, including right premotor cortex, right supramarginal gyrus (SMG), left hippocampus, and right primary motor cortex. Regions negatively correlated with orientation accuracy are not discussed here as we were only interested in regions where increased activity was associated with higher performance.

A post hoc task PLS analysis was carried out to investigate whether the unique patterns of brain activity were related to correct versus noncorrect trails across all participants (i.e., a within-subject effect), rather than being persistent in certain individuals (i.e., a between-subject effect). That is, it may be that the spatiotemporal pattern depicted in Figure 5 is associated with accurate decision-making in all individuals rather than being the pattern expressed by high-performers when making both correct and noncorrect orientation decisions. This task PLS resulted in a nonsignificant LV ($p = .91$), suggesting that the spatiotemporal patterns expressed in the LV from the behavior PLS analysis are stable for high-performing individuals across all trials regardless of accuracy and represent a between-subject effect.

Centrality of Additional Brain Regions Expressed in High-performing Individuals

To evaluate the topological importance of the additional brain regions identified in high-performing individuals through the behavior PLS, a graph theoretical analysis was conducted on resting-state fMRI data to investigate the closeness centrality of those regions within the orientation decision network. An adjacency matrix of ROI-to-ROI Fisher-transformed bivariate correlation measures was computed using 12 dominant positive voxel salience clusters from the task PLS and the four dominant positive voxel salience clusters extracted from the behavior PLS. The closeness centrality for each of the four behavior PLS clusters were

Table 2. Cluster Peaks Correlated with High Accuracy in Making Orientation Decisions

Peak Voxel Location	*x (mm)*	*y (mm)*	*z (mm)*	*BSR*
Dominant Positive Saliences				
Right premotor cortex	42	4	42	4.484
Right SMG	56	−20	26	6.8415
Left hippocampus	−36	−22	−10	4.3709
Right primary motor cortex	24	−22	52	3.753
Dominant Negative Saliences				
Right medial temporal pole	44	20	−34	−13.224
Left middle temporal gyrus	−48	−14	−20	−12.4247
Secondary visual cortex (V2)	−22	−82	−4	−11.0454
Right inferior frontal gyrus	46	0	−42	−7.7132
Right pallidum	24	−10	−4	−7.6839
Right middle temporal gyrus	62	−2	−20	−6.6423
Right middle orbital gyrus	34	54	−10	−6.4729
Right middle occipital gyrus	28	−102	2	−6.3431
Right superior occipital gyrus	28	−92	30	−6.2917
Right medial temporal pole	56	8	−18	−5.9288

Positive BSR clusters reflect areas when activity was positively correlated with behavior. Negative BSR clusters reflect areas when activity was negatively correlated with behavior. Coordinates reported in MNI space.

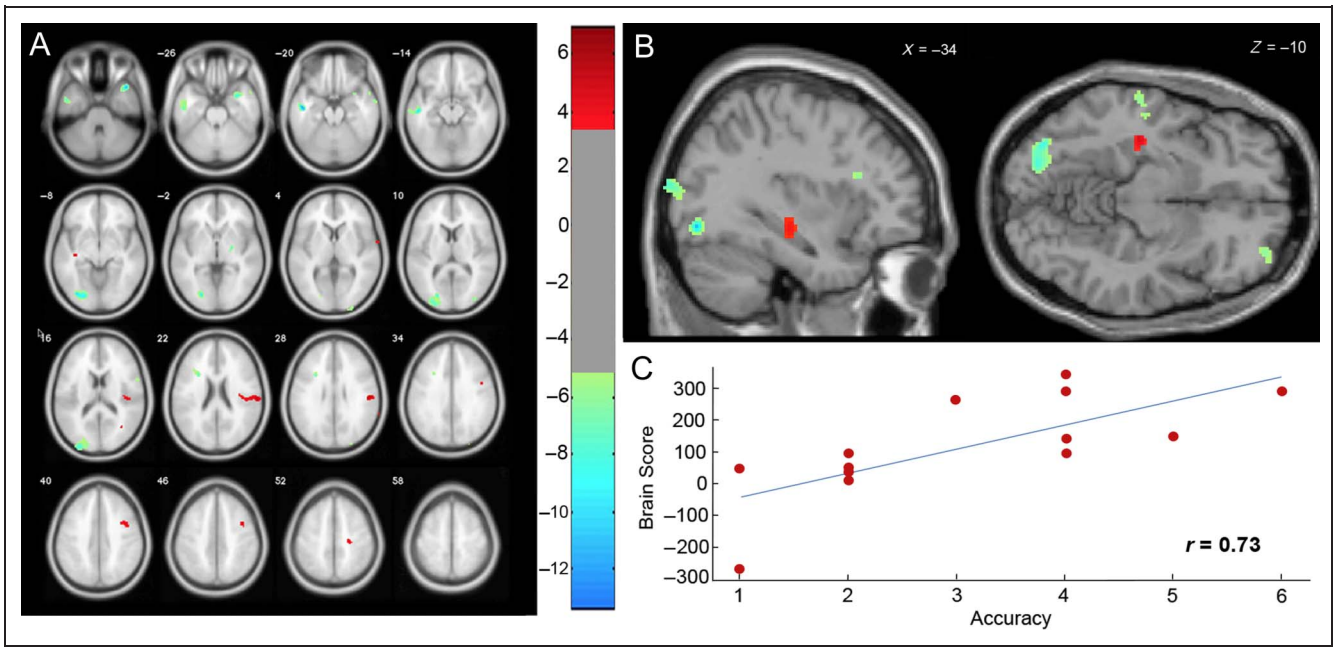

Figure 5. Singular image for the LV ($p < .05$) from the orientation decision behavior PLS. (A) The singular image identifies the distributed network associated with high accuracy in making orientation decisions. Yellow/red regions where increased stable patterns of activity were correlated with high accuracy in the orientation decision task. Blue regions represent regions where stable activity was anticorrelated with orientation accuracy. (B) Sagittal and axial views showing location of cluster within the left hippocampus. (C) Correlation plot showing the relationship between each participant's accuracy on the orientation decision task and their brain scores. Brain scores represent the degree to which each participant shows the spatial pattern of voxels identified in the LV. Displayed in neurological convention (L = L).

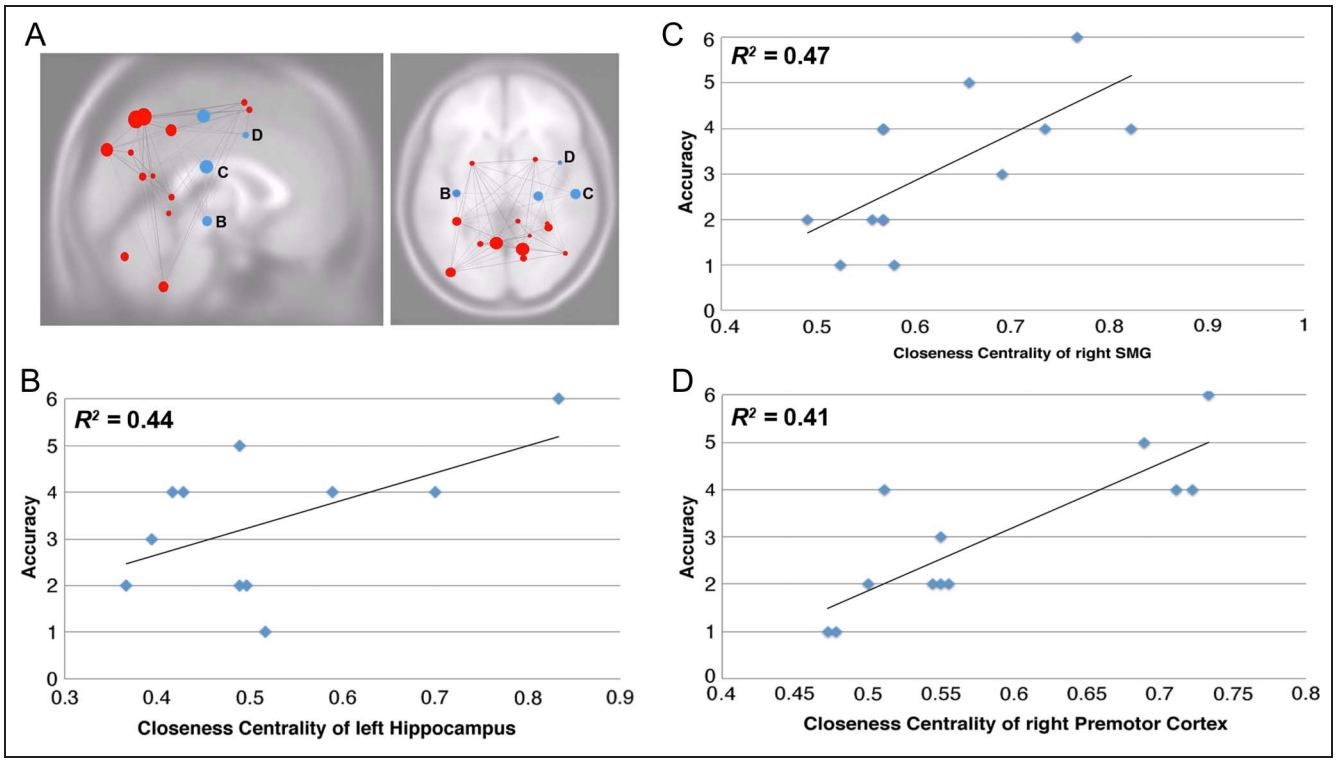

Figure 6. Results from closeness centrality analysis on clusters from the behavior PLS analysis. (A) Axial view of task PLS network with four additional nodes extracted from the behavior PLS analysis. Nodes from behavior PLS analysis with significant relations between closeness centrality and orientation accuracy are labeled B, C, and D. (B) Regression plot for left hippocampus (MNI peak = −36, −22, −10) and orientation accuracy, $t(11) = 2.08$, $p_{FDR} = .049$, $R^2 = 0.44$, with outlier removed ($y = 2, x = 0.07$, Malhalanobis distance = 7.76). (C) Regression plot for right SMG (MNI peak = 56, −20, 26) and orientation accuracy, $t(11) = 3.10$, $p_{FDR} = .019$, $R^2 = 0.47$. (D) Regression plot for right primary motor cortex (MNI peak = 24, −22, 52) and accuracy, $t(9) = 2.77$, $p_{FDR} = .02$, $R^2 = 0.41$.

then calculated. Note that the threshold criterion applied to obtain small-world properties necessitated the exclusion of one participant from the centrality analysis on the cluster from the right premotor cortex and two participants from the cluster in the right primary motor cortex, as these individuals did not have connectivity values exceeding the Fisher transformed $r > 0.15$ threshold. These results are summarized in Figure 6. The closeness centrality of the cluster within the left hippocampus (MNI peak = −36, −22, −10), $t(11) = 2.08$, $p_{FDR} = .049$, $R^2 = 0.28$, the right SMG (MNI peak = 56, −20, 26), $t(11) = 3.10$, $p_{FDR} = .019$, $R^2 = 0.47$, and the right primary motor cortex (MNI peak = 24, −22, 52), $t(9) = 2.77$, $p_{FDR} = .02$, $R^2 = 0.41$, were found to be significantly related to accuracy on the orientation decision task. The cluster in the right premotor cortex (MNI peak = 42, 4, 42) was not significantly related to orientation accuracy, $t(10) = 0.92$, $p_{FDR} = .19$, $R^2 = 0.07$. These results show that the majority of brain areas identified through the behavior PLS are more topologically central at rest in high-performing individuals. This suggests that increased centrality provides a measure of the ability of a region to participate in a task network, which may facilitate performance of behaviors that rely on those networks.

DISCUSSION

The findings described in this study are consistent with a growing number of studies on the relevance of properties of neural networks in influencing human behavior (Breakspear & McIntosh, 2011). Within the context of human spatial orientation, we provide evidence for two sources of network variability in shaping the ability to orient in spatial surroundings: variation in the configuration of task-evoked networks engaged while making orientation decisions and the intrinsic, task-independent integrative capacity of those network elements measured through resting-state signal. The first source of variability—task-evoked network configuration—suggests that individual differences in which brain regions are recruited into task-evoked networks strongly relates to the performance of behaviors relying on those networks. Critically, it was found that high-performing individuals engaged additional brain areas during the orientation task that have been shown to be involved in spatial processing, suggesting that their inclusion into the task network conferred a behavioral advantage over low performing individuals. The second source of variability—task-independent integrative capacity—suggests that topological variability in the capacity of brain networks to integrate information processed in different network nodes contributes to the expression of behaviors and cognitive processes that rely on those networks. Taken together, these results support a model of brain organization in which behavior is modulated by the ability to configure functional networks based on task demands (McIntosh, 2000, 2004) and by the underlying functional connections of those elements forming the network.

To understand how network configuration relates to the ability to spatially orient, we performed a task PLS and a behavior PLS on data collected while participants solved an orientation decision task. The task PLS identified a core group of brain regions across the entire group of participants that displayed increased activity while making orientation decisions. These activations are in line with processing streams outlined in previous computational models of spatial memory (Byrne et al., 2007; Burgess, Becker, et al., 2001; Burgess, Maguire, Spiers, & O'Keefe, 2001). Early sensory information is fed forward through the posterior parietal cortex to the parahippocampal cortex, a region that supports landmark recognition through firing properties of so called "view cells" (Ekstrom et al., 2003). The parahippocampal cortex establishes a location within the environment based on the angular direction to the landmark and its position within the viewable environmental context. This information is hypothesized in the computational models to be used by the RSC, which translates allocentric scene/viewpoint spatial information and egocentric body centered information processed in the precuneus (Vann, Aggleton, & Maguire, 2009; Iaria, Chen, Guariglia, Ptito, & Petrides, 2007) for the purpose of route planning (Spiers & Maguire, 2006). The output of this integrative processing in the RSC is then fed forward to regions in the left and right precentral gyrus—areas that have been found to translate spatial representations into motor intentions (Ikkai & Curtis, 2011)—for the purpose of making orientation decisions.

The results of this study contribute to these models by providing evidence that variability in the configuration of this network relates to the capacity of an individual to correctly spatially orient. In addition to the core network shared by the entire group, high-performers showed increased activity within the right SMG, which has been associated with the generation (de Borst et al., 2012; Medina et al., 2009; Knauff, Kassubek, Mulack, & Greenlee, 2000) and manipulation (Sack et al., 2002) of egocentric-based spatial imagery as well as visuospatial working memory (Silk, Bellgrove, Wrafter, Mattingley, & Cunnington, 2010; Geier, Garver, & Luna, 2007). Increased activity was also detected in the left hippocampus, an area that is crucial for representing the spatial layout of an environment (Hassabis & Maguire, 2007; Iaria et al., 2007), route planning (Spiers & Maguire, 2006), and temporally sequencing scenes for the purpose of navigation (Iglói, Doeller, Berthoz, Rondi-Reig, & Burgess, 2010). The engagement of these regions did not vary based on accuracy within each trial. Instead, they appear to be general features of an individual's brain response to the demands of our task that confer a behavioral advantage over people who did not express those patterns.

As our orientation decision task required participants to situate perspective-based egocentric reference frames into the spatial context of a virtual environment that codes

the relationship between environmental landmarks, we believe the inclusion of these regions in the differential configuration of task-based brain networks facilitated a participant's ability twofold. First, through increased engagement of the left hippocampus, high-performing individuals may have been better able to mentally represent their location by coordinating and integrating information processed throughout the medial-temporal lobes to generate the spatial context of the environment. Second, through the increased engagement of the right SMG, high-performing individuals may have been more flexibly in manipulating the spatial scene to make accurate orientation decisions based on the spatial processing occurring in parietal, RSC, and medial-temporal lobe systems that were common to the whole group of participants. Areas in the right premotor and motor cortex have been shown to increase activity in spatial tasks with working memory and motor intention demands (Ikkai & Curtis, 2011), suggesting that their inclusion in the high-performing individuals supported the generation of an accurate motor attention based on the orientation decision made during the task.

The second source of neural variability investigated in this study is the degree of global efficiency within a resting-state network that was composed of brain regions we found to be engaged during the orientation task. Here, we found a strong correlation between the global efficiency of the task-defined network during rest and accuracy in making orientation decisions. As global efficiency is believed to quantify the capacity for parallel information transfer and integrated processing (Bullmore & Sporns, 2009; van den Heuvel & Hulshoff Pol, 2010; Sporns et al., 2007), these results suggest that the integrative capacity of the task-defined orientation network modulated the degree to which an individual was able to intrinsically coordinate and synchronize the neural activity while making orientation decisions, which ultimately related to the accuracy of their response. Our finding that each participant was able to freely reproduce the spatial layout of the testing environment following a 20–40 min delay suggests that individual variability in the ability to spatially orient is not related to a person's capacity to remember the composition of an environment per se but appears to be related to their ability to dynamically integrate spatial information from within their immediate environment and with information encoded in memory. On the basis of these results, we suggest that global efficiency of task-related networks measured at rest may provide an index of the cognitive capacity of processes that rely on those networks. Critically, we also observed that the global efficiency values derived from the task-related network were only predictive of performance on our orientation decision task and not on the facial identity task or an emotion recognition task. This suggests that our results are specific to the orientation decision process and do not appear to generalize to other nonspatial perceptual tasks.

We further investigated the topographic relationship of the additional four brain areas identified in the behavior PLS to the whole group network constructed from the task PLS results. We found that the left hippocampus, right SMG, and right primary motor cortex clusters identified in the behavior PLS had a higher degree of closeness centrality within the task-related network of participants that were more accurate on the orientation decision task. Previous research has provided evidence for the role of the hippocampus in the use of allocentric representations of space to flexibly and efficiently navigate through environments (Marchette et al., 2011; Jeewajee, Barry, O'Keefe, & Burgess, 2008; Wolbers, Wiener, Mallot, & Büchel, 2007; Hartley et al., 2003; Iaria et al., 2003; Maguire et al., 1998), as well as integrating neural firing associated with spatial processing in the medial entorhinal cortex and parahippocampal cortex to generate a sense of location within an environment (Begega et al., 2012; Burgess & O'Keefe, 2011; Derdikman & Moser, 2010; Hartley, Burgess, Lever, Cacucci, & O'Keefe, 2000; O'Keefe & Burgess, 1996). Although the hippocampus is commonly engaged during tasks using allocentric spatial information, its position as the primary structure in generating spatial representations remains actively debated; past research has shown that some forms of allocentric-based spatial memories can persist in the presence of hippocampal lesions (Bohbot et al., 1998) and that the place representations generated by hippocampal place cells may be only one part of a broader circuit throughout the medial-temporal lobes that is used to understand self-location within an environment (Moser, Kroff, & Moser, 2008). The results from this study support the network-based perspective by showing that increased centrality of the left hippocampus within a brain network at rest that is engaged during spatial orientation affords more accurate orientation. This may result from an increased capacity of the hippocampus to communicate with other spatially relevant brain regions throughout the medial-temporal lobes and frontal and parietal cortex to help establish a representation of place within an allocentric environmental reference frame and use it to correctly guide orientation decisions. This hypothesis is additionally supported by the relationship between the centrality of the rSMG and orientation accuracy, as the rSMG has been associated with spatial working memory (Ikkai & Curtis, 2011; Geier et al., 2007) and spatial attention (Silk et al., 2010), both of which are critical components for complex spatial behaviors such as orientation.

At a general systems level, it is interesting to further speculate on the functional importance of node centrality within brain networks. In this study, increased centrality of three of the four clusters identified through the behavior PLS nodes were related to increases in orientation accuracy. Although we are unable to directly assess this, it may be that the increased functional coupling between the node and the other network elements during rest influenced its expression during the orientation task for

high-performers. Future research may be able to generate likelihood models of interindividual differences in task-related network configuration based on prior knowledge of the centrality of brain regions within resting-state networks.

There are a few notable limitations in this study. First, the orientation decision task used is novel and has only been reported once before (Arnold et al., 2013). More research is needed to clarify the specific cognitive processes underlying orientation decisions, as the typical approach to studying orientation and navigation has been to conflate decision-making processes with movement through a virtual environment (e. g., Hartley et al., 2003; Iaria et al., 2003; but see Spiers & Maguire, 2006, for an attempt to disambiguate these two components). Second, nodes within the task-related networks are only characterized by one measure of centrality. Although the closeness centrality of nodes within multimodal regions such as the hippocampus has been shown to intersect with other topological properties of nodes such as degree, motif fingerprint, and betweenness centrality (Sporns et al., 2007), more research is needed to fully delineate the commonalities and unique aspects of network topologies in the brain that each measure quantifies.

In summary, our results present a novel view on the role of neural network variability in influencing a person's ability to spatially orient. Our findings indicate that both neural network configuration and integration underlie the ability to accurately orient using environmental features in large-scale environments. As participants could reproduce the location of each landmark after a 20- to 40-min time delay with 100% accuracy, this suggests that individual variability in spatial orientation is not necessarily due to inaccuracies or errors in spatial encoding but is related to the dynamic configuration and capacity for integration of spatial information within the neurocognitive network that underlies spatial orientation ability. The combination of PLS and graph metrics provides a means to assess topological variability in brain networks underlying complex cognitive skills, as it allows researchers to model interindividual differences in the expression and processing efficiency of task-related brain networks. Importantly, these results have potential clinical extensions to understand and detect early symptoms of neurodegenerative disorders such as Alzheimer's disease (AD) that are known to be associated with topographical disorientation (Pengas et al., 2012; Bird et al., 2009; Iachini, Iavarone, Senese, Ruotolo, & Ruggiero, 2009; deIpolyi, Rankin, Mucke, Miller, & Gorno-Tempini, 2007). In such a case, the disease may alter neural dynamics within spatial memory networks before clear clinical symptoms of the neurodegeneration in specific brain regions become apparent (Smith, Clithero, Rorden, & Karnath, 2013). Future studies would benefit from investigating how topological components of spatial orientation networks change in the context of neurodegenerative disorders and whether these changes are indicative of clinical severity and predictive of further cognitive decline.

Acknowledgments

We thank the staff members of the Neuroimaging Research Unit at the Seaman Family MR Research Centre for their technical support. This research was financially supported by the Natural Sciences and Engineering Research Council of Canada to G. I. (RT735872). A. A. was supported by Alberta Health Services and the Ministry of Human Services as a part of the Collaborative Research Grant Initiative: Mental Wellness in Seniors and Persons with Disabilities. S. B. was supported by an NSERC PDF and iCore.

Reprint requests should be sent to Aiden E. G. F. Arnold, University of Calgary, 2500 University Drive NW, Calgary, Alberta, Canada, T2N 1N4, or via e-mail: aarnold@ucalgary.ca.

Note

1. The total number of video clips presented was determined from the results of a pilot behavioral study (Arnold et al., 2013), in which we found that participants (similar in age and gender to participants in the current study) were able to form a correct mental representation of a virtual city with four unique landmarks by the end of the eighth trial on average.

REFERENCES

Archard, S., & Bullmore, E. (2007). Efficiency and cost of economical brain functional networks. *PLoS Computational Biology, 3,* 174–183.

Arleo, A., & Rondi-Reig, L. (2007). Multimodal sensory integration and concurrent navigation strategies for spatial cognition in real and artificial organisms. *Journal of Integrative Neuroscience, 6,* 327–366.

Arnold, A. E. G. F., Burles, F., Krivoruchko, T., Liu, I., Rey, C. D., Levy, R. M., et al. (2013). Cognitive mapping in humans and its relationship to other orientation skills. *Experimental Brain Research, 224,* 359–372.

Baldassarre, A., Lewis, C. M., Committeri, G., Snyder, A. Z., Romani, G. L., & Corbetta, M. (2012). Individual variability in functional connectivity predicts performance of a perceptual task. *Proceedings of the National Academy of Sciences, U.S.A., 109,* 3516–3521.

Bassett, D. S., & Bullmore, E. (2006). Small-world brain networks. *Neuroscientist, 12,* 512–523.

Begega, A., Cuesta, M., Rubio, S., Méndez, M., Santín, L. J., & Arias, J. L. (2012). Functional networks involved in spatial learning strategies in middle-aged rats. *Neurobiology of Learning and Memory, 97,* 346–353.

Behzadi, Y., Restom, K., Liau, J., & Liu, T. (2007). A component based noise correction method (CompCor) for BOLD and perfusion based fMRI. *Neuroimage, 37,* 90–101.

Bird, C. M., Chan, D., Hartley, T., Pijnenburg, Y. A., Rossor, M. N., & Burgess, N. (2009). Topographical short-term memory differentiates Alzheimer's disease from frontotemporal lobar degeneration. *Hippocampus, 20,* 1154–1169.

Biswal, B., Mennes, M., Zuo, X. N., Gohel, S., Kelly, C., Smith, S. M., et al. (2010). Toward discovery science of human brain function. *Proceedings of the National Academy of Sciences, U.S.A., 107,* 4734–4739.

Bohbot, V. D., Kalina, M., Stepankova, K., Spackova, N., Petrides, M., & Nadel, L. (1998). Spatial memory deficits in patients with lesions to the right hippocampus and to the right parahippocampal cortex. *Neuropsychologia, 36,* 1217–1238.

Bolognini, N., Olgiati, E., Rossetti, A., & Maravita, A. (2010). Enhancing multisensory spatial orienting by brain polarization

of the parietal cortex. *European Journal of Neuroscience, 31,* 1800–1806.
Breakspear, M., & McIntosh, A. R. (2011). Networks, noise and models: Reconceptualizing the brain as a complex, distributed system. *Neuroimage, 58,* 293–295.
Bullmore, E., & Sporns, O. (2009). Complex brain networks: Graph theoretical analysis of structural and functional systems. *Nature Reviews Neuroscience, 10,* 186–198.
Burgess, N. (2008). Spatial cognition and the brain. *Annals of the New York Academy of Sciences, 1124,* 77–97.
Burgess, N., Becker, S., King, J. A., & O'Keefe, J. (2001). Memory for events and their spatial context: Models and experiments. *Philosophical Transactions of the Royal Society of London, Series B, Biological Sciences, 356,* 1493–1503.
Burgess, N., Maguire, E. A., Spiers, H. J., & O'Keefe, J. (2001). A temporoparietal and prefrontal network for retrieving the spatial context of lifelike events. *Neuroimage, 14,* 439–453.
Burgess, N., & O'Keefe, J. (2011). Models of place and grid cell firing and theta rhythmicity. *Current Opinion in Neurobiology, 21,* 734–744.
Byrne, P., Becker, S., & Burgess, N. (2007). Remembering the past and imagining the future: A neural model of spatial memory and imagery. *Psychological Review, 114,* 340–375.
Chai, X. J., Nieto-Castañón, A., Öngür, D., & Whitfield-Gabrieli, S. (2012). Anticorrelations in resting state networks without global signal regression. *Neuroimage, 59,* 1420–1428.
Corbetta, M., Kincade, J. M., & Shulman, G. L. (2002). Neural systems for visual orienting and their relationships to spatial working memory. *Journal of Cognitive Neuroscience, 14,* 508–523.
de Borst, A. W., Sack, A. T., Jansma, B. M., Esposito, F., de Martino, F., Valente, G., et al. (2012). Integration of "what" and "where" in frontal cortex during visual imagery of scenes. *Neuroimage, 60,* 47–58.
deIpolyi, A. R., Rankin, K. P., Mucke, L., Miller, B. L., & Gorno-Tempini, M. L. (2007). Spatial cognition and the human navigation network in AD and MCI. *Neurology, 69,* 986–997.
Derdikman, D., & Moser, E. I. (2010). A manifold of spatial maps in the brain. *Trends in Cognitive Sciences, 14,* 561–569.
Ekstrom, A. D., Kahana, M. J., Caplan, J. B., Fields, T. A., Isham, E. A., Newman, E. L., et al. (2003). Cellular networks underlying human spatial navigation. *Nature, 425,* 184–188.
Freeman, L. C. (1979). Centrality in social networks: Conceptual clarification. *Social Networks, 1,* 215–239.
Friston, K. J., & Price, C. J. (2001). Dynamic representations and generative models of brain function. *Brain Research Bulletin, 54,* 275–285.
Geier, C. F., Garver, K. E., & Luna, B. (2007). Circuitry underlying temporally extended spatial working memory. *Neuroimage, 35,* 904–915.
Ginestet, C. E., & Simmons, A. (2011). Statistical parametric network analysis of functional connectivity dynamics during a working memory task. *Neuroimage, 55,* 688–704.
Hampson, M., Driesen, N. R., Skudlarski, P., Gore, J. C., & Constable, R. T. (2006). Brain connectivity related to working memory performance. *Journal of Neuroscience, 26,* 13338–13343.
Hartley, T., Burgess, N., Lever, C., Cacucci, F., & O'Keefe, J. (2000). Modeling place fields in terms of the cortical inputs to the hippocampus. *Hippocampus, 10,* 369–379.
Hartley, T., Maguire, E. A., Spiers, H. J., & Burgess, N. (2003). The well-worn route and the path less traveled: Distinct neural bases of route following and wayfinding in humans. *Neuron, 37,* 877–888.
Harvey, C. D., Coen, P., & Tank, D. W. (2012). Choice-specific sequences in parietal cortex during a virtual-navigation decision task. *Nature, 484,* 62–68.
Hassabis, D., & Maguire, E. A. (2007). Deconstructing episodic memory with construction. *Trends in Cognitive Sciences, 11,* 299–306.
Hilgetag, C. C., & Kaiser, M. (2004). Clustering organization of cortical connectivity. *Neuroinformatics, 2,* 353–360.
Iachini, I., Iavarone, A., Senese, V. P., Ruotolo, F., & Ruggiero, G. (2009). Visuospatial memory in healthy elderly, AD and MCI: A review. *Current Aging Science, 2,* 43–59.
Iaria, G., Chen, J., Guariglia, C., Ptito, A., & Petrides, M. (2007). Retrosplenial and hippocampal brain regions in human navigation: Complementary functional contributions to the formation and use of cognitive maps. *European Journal of Neuroscience, 25,* 890–899.
Iaria, G., Petrides, M., Dagher, A., & Pike, B. (2003). Cognitive strategies dependent on the hippocampus and caudate nucleus in human navigation: Variability and change with practice. *Journal of Neuroscience, 23,* 5945–5952.
Iglói, K., Doeller, C. F., Berthoz, A., Rondi-Reig, L., & Burgess, N. (2010). Lateralized human hippocampal activity predicts navigation based on sequence or place memory. *Proceedings of the National Academy of Sciences, U.S.A., 107,* 14466–14471.
Ikkai, A., & Curtis, C. E. (2011). Common neural mechanisms supporting spatial working memory, attention and motor intention. *Neuropsychologia, 49,* 1428–1434.
Iturria-Medina, Y., Canales-Rodriguez, E. J., Melie-Garcia, L., Valdes-Hernandez, P. A., Martinez-Montes, E., Alemán-Gómez, Y., et al. (2007). Characterizing brain anatomical connections using diffusion weighted MRI and graph theory. *Neuroimage, 36,* 645–660.
Iturria-Medina, Y., Sotero, R. C., Canales-Rodriguez, E. J., Aleman-Gomez, Y., & Melie-Garcia, L. (2008). Studying the human brain anatomical network via diffusion-weighted MRI and graph theory. *Neuroimage, 40,* 1064–1076.
Jeewajee, A., Barry, C., O'Keefe, J., & Burgess, N. (2008). Grid cells and theta as oscillatory interference: Electrophysiological data from freely moving rats. *Hippocampus, 18,* 1175–1185.
Knauff, M., Kassubek, J., Mulack, T., & Greenlee, M. W. (2000). Cortical activation evoked by visual mental imagery as measured by fMRI. *NeuroReport, 11,* 3957–3962.
Krishnan, A., Williams, L. J., McIntosh, A. R., & Abdi, H. (2011). Partial least squares (PLS) methods for neuroimaging: A tutorial and review. *Neuroimage, 56,* 455–475.
Latora, V., & Marchiori, M. (2001). Efficient behavior of small-world networks. *Physical Review Letters, 87,* 198701.
Liu, I., Levy, R. M., Barton, J. J. S., & Iaria, G. (2011). Age and gender differences in various topographical orientation strategies. *Brain Research, 1410,* 112–119.
Lundqvist, D., & Litton, J. E. (1998). *The averaged Karolinska directed emotional faces–AKDEF.* CD ROM from Department of Clinical Neuroscience, Psychology Section, Karolinska Institutet, ISBN 91-630-7164-9.
Maguire, E., Burgess, N., Donnett, J., Frackowiak, R., Frith, C., & O'Keefe, J. (1998). Knowing where and getting there: A human navigation network. *Science, 280,* 921–924.
Marchette, S. A., Bakker, A., & Shelton, A. L. (2011). Cognitive mappers to creatures of habit: Differential engagement of place and response learning mechanisms predicts human navigational behavior. *Journal of Neuroscience, 31,* 15264–15268.

McIntosh, A. R. (2000). Towards a network theory of cognition. *Neural Networks, 13,* 861–870.
McIntosh, A. R. (2004). Contexts and catalysts: A resolution of the localization and integration of function in the brain. *Neuroinformatics, 2,* 175–182.
McIntosh, A. R., Bookstein, F. L., Haxby, J. V., & Grady, C. L. (1996). Spatial pattern analysis of functional brain images using partial least squares. *Neuroimage, 3,* 143–157.
Medina, J., Kannan, V., Pawlak, M. A., Kleinman, J. T., Newhart, M., Davis, C., et al. (2009). Neural substrates of visuospatial processing in distinct reference frames: Evidence from unilateral spatial neglect. *Journal of Cognitive Neuroscience, 21,* 2073–2084.
Melie-García, L., Sanabria-Diaz, G., & Sánchez-Catasús, C. (2013). Studying the topological organization of the cerebral blood flow fluctuations in resting state. *Neuroimage, 64,* 173–184.
Moser, E. I., Kroff, E., & Moser, M. B. (2008). Place cells, grid cells, and the brain's spatial representation system. *Annual Review of Neuroscience, 31,* 69–89.
O'Keefe, J., & Burgess, N. (1996). Geometric determinants of the place fields of hippocampal neurons. *Nature, 381,* 425–428.
Pengas, G., Williams, G. B., Acosta-Cabronero, J., Ash, T. W. J., Hong, Y. T., Izquierdo-Garcia, D., et al. (2012). The relationship of topographical memory performance to regional neurodegeneration in Alzheimer's disease. *Frontiers in Aging Neuroscience, 4,* 17.
Rubinov, M., & Sporns, O. (2010). Complex measures of brain connectivity: Uses and interpretations. *Neuroimage, 52,* 1059–1069.
Sack, A. T., Sperling, J. M., Prvulovic, D., Formisano, E., Goebel, R., di Salle, F., et al. (2002). Tracking the mind's image in the brain II: Transcranial magnetic stimulation reveals parietal asymmetry in visuospatial imagery. *Neuron, 35,* 195–204.
Silk, T. J., Bellgrove, M. A., Wrafter, P., Mattingley, J. B., & Cunnington, R. (2010). Spatial working memory and spatial attention rely on common neural processes in the intraparietal sulcus. *Neuroimage, 53,* 718–724.
Smith, D. V., Clithero, J. A., Rorden, C., & Karnath, H. O. (2013). Decoding the anatomical network of spatial attention. *Proceedings of the National Academy of Sciences, U.S.A., 110,* 1518–1523.
Spiers, H. J., & Maguire, E. A. (2006). Thoughts, behaviour, and brain dynamics during navigation in the real world. *Neuroimage, 31,* 1826–1840.
Sporns, O., Honey, C. J., & Kötter, R. (2007). Identification and classification of hubs in brain networks. *PLoS One, 2,* e1049.
Sporns, O., Tononi, G., & Edelman, G. M. (2000). Theoretical neuroanatomy: Relating anatomical and functional connectivity in graphs and cortical connection matrices. *Cerebral Cortex, 10,* 127–141.
van den Heuvel, M. P., & Hulshoff Pol, H. E. (2010). Exploring the brain network: A review on resting-state fMRI functional connectivity. *Eur Neuropsychopharmacol, 20,* 519–534.
van den Heuvel, M. P., Stam, C. J., Kahn, R. S., & Hulshoff Pol, H. E. (2009). Efficiency of functional brain networks and intellectual performance. *Journal of Neuroscience, 29,* 7619–7624.
Vann, S. D., Aggleton, J. P., & Maguire, E. A. (2009). What does the retrosplenial cortex do? *Nature Reviews Neuroscience, 10,* 792–802.
Watts, D. J., & Strogatz, S. H. (1998). Collective dynamics of "small-world" networks. *Nature, 393,* 440–442.
Wegman, J., & Janzen, G. (2011). Neural encoding of objects relevant for navigation and resting state correlations with navigational ability. *Journal of Cognitive Neuroscience, 23,* 3841–3854.
Whitfield-Gabrieli, S., & Nieto-Castanon, A. (2012). Conn: A functional connectivity toolbox for correlated and anticorrelated brain networks. *Brain Connectivity, 2,* 125–141.
Wolbers, T., & Büchel, C. (2005). Dissociable retrosplenial and hippocampal contributions to successful formation of survey representations. *Journal of Neuroscience, 25,* 3333–3340.
Wolbers, T., & Hegarty, M. (2010). What determines our navigational abilities? *Trends in Cognitive Sciences, 14,* 138–146.
Wolbers, T., Wiener, J. M., Mallot, H. A., & Büchel, C. (2007). Differential recruitment of the hippocampus, medial prefrontal cortex, and the human motion complex during path integration in humans. *Journal of Neuroscience, 27,* 9408–9416.